

# Chapter 1

## Infrared Detector Characterization

Over the past several hundreds of years, optical systems (telescopes, microscopes, eyeglasses, cameras, etc.) have formed their optical image on the human retina, photographic plate, or film. The birth of photodetectors dates back to 1873 when Smith discovered photoconductivity in selenium. Progress was slow until 1905, when Einstein explained the newly observed photoelectric effect in metals, and Planck solved the blackbody emission puzzle by introducing the quantum hypothesis. Applications and new devices soon flourished, pushed by the dawning technology of vacuum tube sensors developed in the 1920s and 1930s, culminating in the advent of television. Zworykin and Morton, the celebrated fathers of videonics, on the last page of their legendary book *Television* (1939) concluded that: “*when rockets will fly to the moon and to other celestial bodies, the first images we will see of them will be those taken by camera tubes, which will open to mankind new horizons.*” Their foresight became a reality with the Apollo and Explorer missions. Photolithography enabled the fabrication of silicon monolithic imaging focal planes for the visible spectrum beginning in the early 1960s. Some of these early developments were intended for a videophone, and other efforts were for television cameras, satellite surveillance, and digital imaging. Infrared imaging has been vigorously pursued in parallel with visible imaging because of its utility in military applications. More recently (1997), the charged-coupled device (CCD) camera aboard the Hubble Space Telescope delivered a deep-space picture, a result of 10 day’s integration, featuring galaxies of the 30<sup>th</sup> magnitude—an unimaginable figure, even for astronomers of our generation. Thus, photodetectors continue to open to humanity the most amazing new horizons.

### 1.1 Introduction

Many materials have been investigated in the infrared (IR) field. Figure 1.1 gives approximate dates of significant developmental efforts for infrared

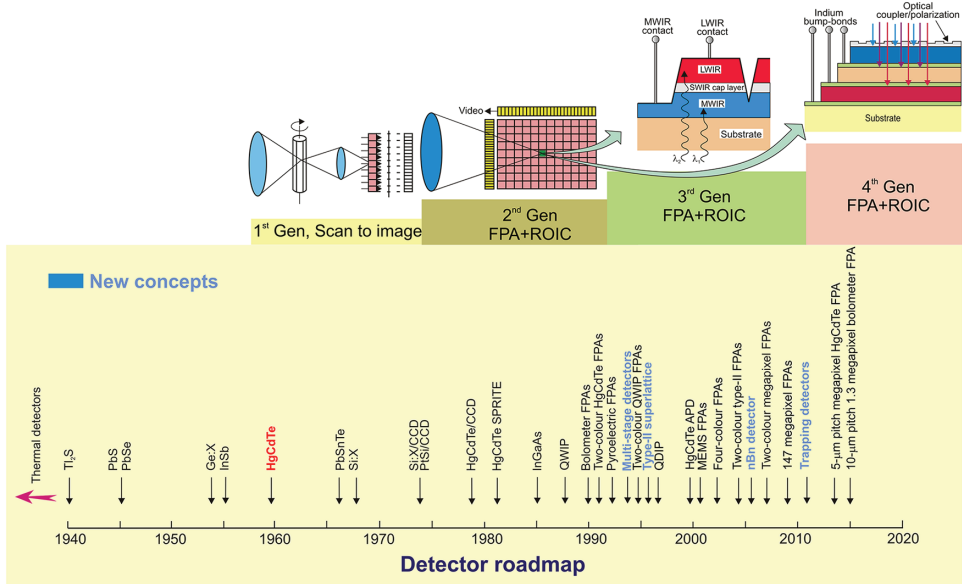


**Figure 1.1** History of the development of infrared detectors and systems. New concepts of detectors developed in last two decades are marked in blue. Four generations of systems can be considered for principal military and civilian applications: first generation (scanning systems), second generation (staring systems with electronic scanning), third generation (staring systems with a large number of pixels and two-color functionality), and fourth generation (staring systems with a very large number of pixels, multi-color functionality, and other on-chip functions; e.g., better radiation/pixel coupling, avalanche multiplication in pixels, and polarization/phase sensitivity) (adapted from Ref. 3).

materials. During the 1950s, IR detectors were built using single-element-cooled lead salt photodetectors, primarily for anti-air-missile seekers. Usually lead salt detectors were polycrystalline and were produced by vacuum evaporation and chemical deposition from a solution, followed by a post-growth sensitization process.<sup>1</sup> The first extrinsic photoconductive detectors were reported in the early 1950s<sup>2</sup> after the discovery of the transistor, which stimulated a considerable improvement and growth of material purification techniques. Since the techniques for controlled impurity introduction became available for germanium at an earlier date, the first high-performance extrinsic detectors were based on Ge:Hg with activation energy for the Hg acceptor of 0.089 eV. Extrinsic photoconductive response from copper, zinc, and gold impurity levels in germanium gave rise to devices using the 8- to 14- $\mu$ m long wavelength IR (LWIR) spectral window and beyond to the 14- to 30- $\mu$ m very long wavelength IR (VLWIR) region.

In 1967 the first comprehensive extrinsic Si detector-oriented paper was published by Soref.<sup>4</sup> However, the state of extrinsic Si was not changed significantly. Although Si has several advantages over Ge (namely, a lower dielectric constant giving shorter dielectric relaxation time and lower capacitance, higher dopant solubility and larger photoionization cross section for higher quantum

efficiency, and lower refractive index for lower reflectance), these were not sufficient to warrant the necessary development efforts needed to bring it to the level of the, by then, highly developed Ge detectors. After being dormant for about ten years, extrinsic Si was reconsidered after the invention of CCDs by Boyle and Smith.<sup>5</sup> In 1973, Shepherd and Yang<sup>6</sup> proposed the metal-silicide/silicon Schottky barrier detectors. For the first time it became possible to have much more sophisticated readout schemes—both detection and readout could be implemented in one common silicon chip.

At the same time, rapid advances were being made in narrow bandgap semiconductors that would later prove useful in extending wavelength capabilities and improving sensitivity. The fundamental properties of narrow-gap semiconductors (high optical absorption coefficient, high electron mobility and low thermal generation rate), together with the capability for bandgap engineering, make these alloy systems almost ideal for a wide range of IR detectors. The first such material was InSb,<sup>7</sup> a member of the newly discovered III-V compound semiconductor family, but its operation is limited to the mid-wavelength IR (MWIR) spectral range. The perceived requirement for detection in LWIR band led to development of narrow-gap ternary alloy systems such as InAsSb, PbSnTe, and HgCdTe.<sup>8–10</sup>

For 10 years during the late 1960s to the mid-1970s, HgCdTe alloy detectors were in serious competition with IV-VI alloy devices (mainly PbSnTe) for developing photodiodes because of the latter's production and storage problems.<sup>9</sup> However, development of PbSnTe photodiodes was discontinued because the chalcogenides suffered from two significant drawbacks: very high thermal coefficient of expansion (a factor of 7 higher than Si) and short Shockley–Read–Hall (SRH) carrier lifetime. A large thermal coefficient of expansion lead to failure of the indium bonds in hybrid structure (between silicon readout and the detector array) after repeated thermal cycling from room temperature to the cryogenic temperature of operation. In addition, the high dielectric constant of PbSnTe ( $\sim 500$ ) resulted in  $RC$ -response times that were too slow for LWIR scanning systems under development at that time. However, for two-dimensional (2D) staring imaging systems, which are currently under development, this would not be such a significant issue.

HgCdTe has inspired the development of the four “generations” of detector devices (see Fig. 1.1). In the late 1960s and early 1970s, first-generation linear photoconductor arrays were developed. The first generation scanning system does not include multiplexing functions in the infrared focal plane (IRFP). In the mid-1970s attention turned to the photodiodes for passive IR imaging applications. In contrast to photoconductors, photodiodes with their very low power dissipation, inherently high impedance, negligible  $1/f$  noise, and easy multiplexing on a focal plane silicon chip, can be assembled in 2D arrays containing more than megapixel elements, limited only by existing technologies. After the invention of CCDs by Boyle and Smith,<sup>5</sup> the idea of an all-solid-state electronically scanned 2D IR detector array caused attention to be turned to

HgCdTe photodiodes. In the end of the 1970s the emphasis was directed toward large photovoltaic HgCdTe arrays in the MWIR and LWIR spectral bands for thermal imaging. Recent efforts have been extended to short wavelengths, e.g., for starlight imaging in the short wavelength IR (SWIR) range, as well as to VLWIR spaceborne remote sensing beyond 15  $\mu\text{m}$ .

The third-generation HgCdTe and type-II superlattice (T2SL) systems continue to be developed, and concept development towards the so-called fourth generation systems was also recently initiated. The definition of fourth-generation systems is not well established. These systems provide enhanced capabilities in terms of greater number of pixels, higher frame rates, and better thermal resolution, as well as multicolor functionality and other on-chip functions. Multicolor capabilities are highly desirable for advanced IR systems. Collection of data in distinct IR spectral bands can discriminate for both the absolute temperature and the unique signature of objects within the scene. By providing this new dimension of contrast, multiband detection also offers advanced color processing algorithms to further improve sensitivity compared to that of single-color devices. It is expected that the functionalities of fourth-generation systems could manifest themselves as spectral, polarization, phase, or dynamic range signatures that could extract more information from a given scene.<sup>11</sup>

At the beginning of the 1990s, several national agencies (e.g., in U.S., Germany, and France) switched their research emphasis to III-V low-dimensional solid materials (quantum wells and superlattices), as an alternative technology option to HgCdTe, to attain their stated goal of inexpensive large-area IR focal plane arrays (FPAs) amenable to fabrication by the horizontal integration of material foundries and processing centers of excellence. There has been considerable progress towards the materials development and device design innovations. Several new concepts for improvement of the performance of photodetectors have been proposed (see bottom part of Fig. 1.1), where approximate data of significant development efforts are marked in blue. In particular, significant advances have been made in the bandgap engineering of various compound III-V semiconductors that has led to new detector architectures. New emerging strategies include T2SLs, barrier structures such as nBn detectors with lower generation-recombination leakage mechanisms, photon trapping detectors, and multi-stage/cascade infrared devices. The barrier-structure detector concept has recently been applied to resurrect the performance of III-V FPAs, allowing them to operate at considerably higher temperatures than their photodiode counterparts simply by the elimination of depletion regions in the absorber volume. At present, the trade-offs between both competing III-V and II-VI IR materials technologies is observed. It is expected that these two significant schools of thought with regard to the ultimate in photon detection, namely, operation at room temperature, might play a crucial role in the future developments.

## 1.2 Classification of Infrared Detectors

Optical radiation is considered to be radiation ranging from vacuum ultraviolet to submillimeter wavelengths (25 nm to 3000  $\mu\text{m}$ ). The terahertz (THz) region of electromagnetic spectrum (see Fig. 1.2) is often described as the final unexplored area of the spectrum and still presents a challenge for both electronic and photonic technologies. It is frequently treated as the spectral region within the frequency range of  $\nu \approx 0.1\text{--}10$  THz ( $\lambda \approx 3$  mm – 30  $\mu\text{m}$ ) and is partly overlapping with the loosely treated submillimeter (sub-mm) wavelength band  $\nu \approx 0.1\text{--}3$  THz ( $\lambda \approx 3$  mm – 100  $\mu\text{m}$ ).

The majority of optical detectors can be classified in two broad categories: photon detectors (also called quantum detectors) and thermal detectors.

### 1.2.1 Photon detectors

In photon detectors the radiation is absorbed within the material by interaction with electrons either bound to lattice atoms or to impurity atoms or with free electrons. The observed electrical output signal results from the changed electronic energy distribution. The fundamental optical excitation processes in semiconductors are illustrated in Fig. 1.3. In quantum wells [Fig. 1.3(b)] the intersubband absorption takes place between the energy levels of a quantum well associated with the conduction band (n-doped) or valence band (p-doped). In the case of type-II InAs/GaSb superlattice [Fig. 1.3(c)] the superlattice bandgap is determined by the energy difference between the electron miniband E1 and the first heavy-hole state HH1 at the Brillouin zone center. A consequence of the type-II band alignment is spatial separation of electrons and holes.

Relative response of infrared detectors is plotted as a function of wavelength with either a vertical scale of  $W^{-1}$  or photon $^{-1}$  (see Fig. 1.4). The

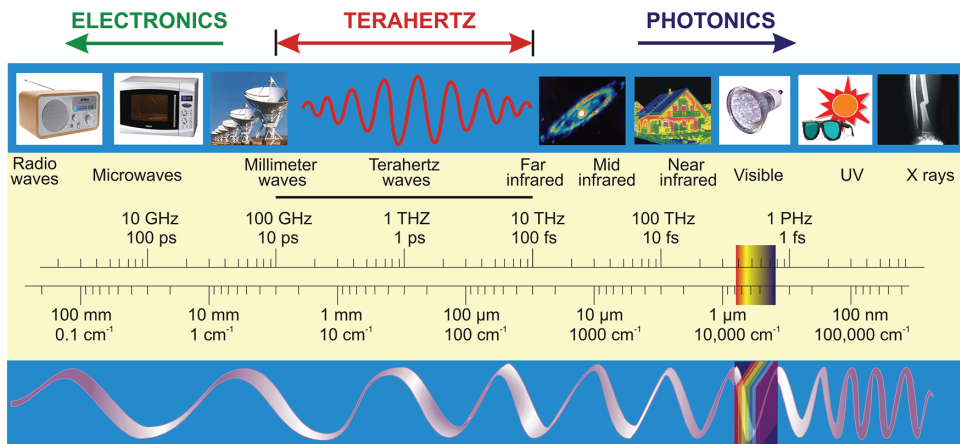
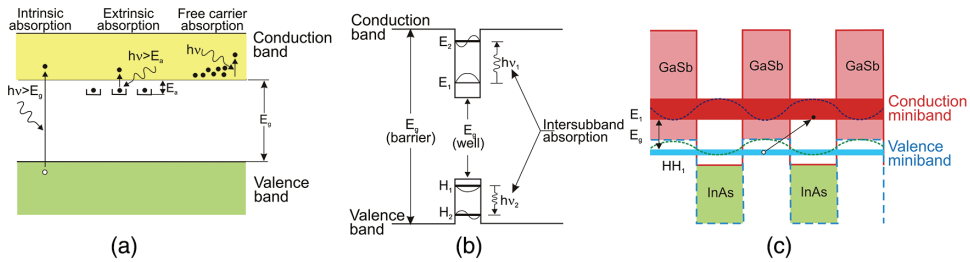
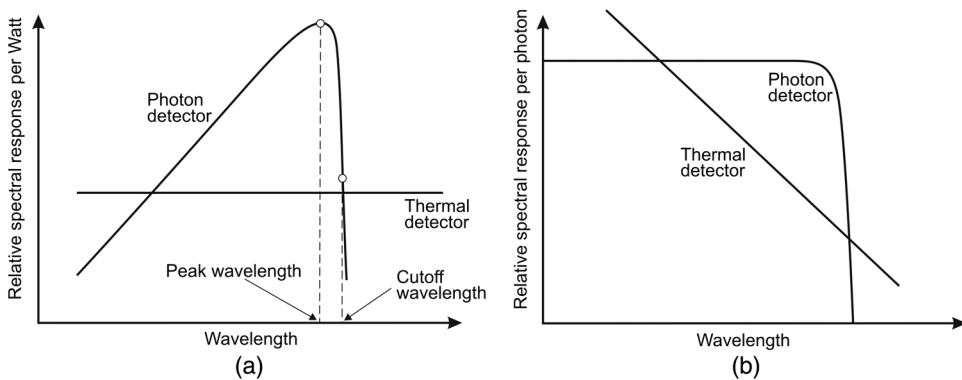


Figure 1.2 The electromagnetic spectrum (adapted from Ref. 12).



**Figure 1.3** Optical excitation processes in: (a) bulk semiconductors, (b) quantum wells, and (c) type-II InAs/GaSb superlattices.



**Figure 1.4** Relative spectral response for a photon and thermal detector for (a) constant incident radiant power and (b) photon flux, respectively.

photon detectors show a selective wavelength dependence of response per unit incident radiation power. Their response is proportional to the rate of arrival photons as the energy per photon is inversely proportional to wavelength. In consequence, the spectral response increases linearly with increasing wavelength [see Fig. 1.4(a)], until the cutoff wavelength is reached, which is determined by the detector material. The cutoff wavelength is usually specified as the long wavelength point at which the detector responsivity falls to 50% of the peak responsivity.

Thermal detectors tend to be spectrally flat in the first case (their response is proportional to the energy absorbed), thus they exhibit a flat spectral response [see Fig 1.4(a)], while photon detectors are generally flat in the second case [see Fig. 1.4(b)].

Photon detectors exhibit both good signal-to-noise performance and a very fast response. But to achieve this, the photon IR detectors may require cryogenic cooling. This is necessary to prevent the thermal generation of charge carriers. The thermal transitions compete with the optical ones, making non-cooled devices very noisy.

Depending on the nature of the interaction, the class of photon detectors is further sub-divided into different types. The most important are: intrinsic detectors, extrinsic detectors, and photoemissive detectors (Schottky barriers).<sup>3</sup> Different types of detectors are briefly characterized in Table 1.1.

A key difference between intrinsic and extrinsic detectors is that extrinsic detectors require much cooling to achieve high sensitivity at a given spectral response cutoff in comparison with intrinsic detectors. Low-temperature operation is associated with longer-wavelength sensitivity in order to suppress noise due to thermally induced transitions between close-lying energy levels.

There is a fundamental relationship between the temperature of the background viewed by the detector and the lower temperature at which the detector must operate to achieve background-limited performance (BLIP). HgCdTe photodetectors with a cutoff wavelength of 12.4  $\mu\text{m}$  operate at 77 K. One can scale the results of this example to other temperatures and cutoff wavelengths by noting that for a given level of detector performance,  $T\lambda_c \approx \text{constant}$ ;<sup>13</sup> i.e., the longer  $\lambda_c$ , the lower is  $T$  while their product remains roughly constant. This relation holds because quantities that determine detector performance vary mainly as an exponential of  $E_{exc}/kT = hc/kT\lambda_c$ , where  $E_{exc}$  is the excitation energy,  $k$  is Boltzmann's constant,  $h$  is Planck's constant, and  $c$  is the velocity of light.

The long wavelength cutoff can be approximated as

$$T_{\max} = \frac{300\text{K}}{\lambda_c[\mu\text{m}]} \quad (1.1)$$

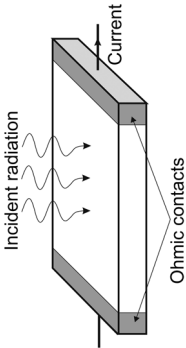
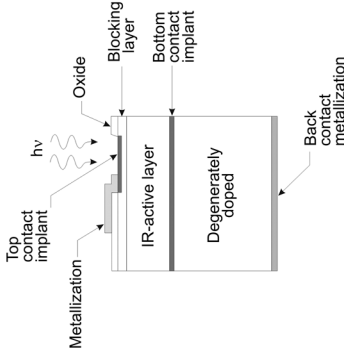
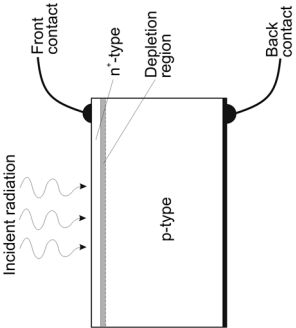
The general trend is illustrated in Fig. 1.5 for six high-performance detector materials suitable for low-background applications: Si, InGaAs, InSb, HgCdTe photodiodes, and Si:As blocked impurity band (BIB) detectors; and extrinsic Ge:Ga unstressed and stressed detectors. Terahertz photoconductors are operated in extrinsic mode.

The most widely used photovoltaic detector is the p–n junction, where a strong internal electric field exists across the junction even in the absence of radiation. Photons incident on the junction produce free hole–electron pairs that are separated by the internal electric field across the junction, causing a change in voltage across the open-circuit cell or a current to flow in the short-circuited case. Due to the absence of recombination noise, the limiting p–n junction's noise level can ideally be  $\sqrt{2}$  times lower than that of the photoconductor.

Photoconductors that utilize excitation of an electron from the valence to conduction band are called intrinsic detectors. Instead those that operate by exciting electrons into the conduction band or holes into the valence band from impurity states within the band (impurity-bound states in energy gap, quantum wells, or quantum dots), are called extrinsic detectors. A key

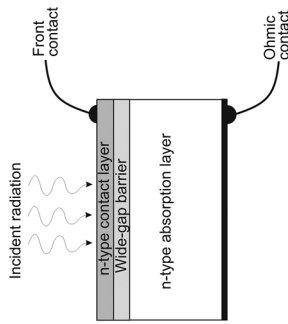


Table 1.1 Photon detectors.

Mode of operation	Schematic of detector	Operation and properties
Photoconductor		<p>This is essentially a radiation-sensitive resistor, generally a semiconductor, either in thin film or bulk form. A photon may release an electron-hole pair or an impurity-bound charge carrier, thereby increasing the electrical conductivity. In almost all cases the change in conductivity is measured by means of electrodes attached to the sample. For low-resistance material, the photoconductor is usually operated in a constant current circuit. For high-resistance photoconductors, a constant voltage circuit is preferred, and the signal is detected as a change in current in the bias circuit.</p>
Blocked impurity band (BIB) detector		<p>The active region of a BIB detector structure, usually based on epitaxially grown n-type material, is sandwiched between a higher-doped degenerate substrate electrode and an undoped blocking layer. Doping of the active layer is high enough for the onset of an impurity band in order to display a high quantum efficiency for impurity ionization (in the case of Si:As BIB, the active layer is doped to <math>\approx 5 \times 10^{17} \text{ cm}^{-3}</math>). The device exhibits a diode-like characteristic, except that photoexcitation of electrons takes place between the donor impurity and the conduction band. The heavily doped n-type IR-active layer has a small concentration of negatively charged compensating acceptor impurities. In the absence of an applied bias, charge neutrality requires an equal concentration of ionized donors. Whereas the negative charges are fixed at acceptor sites, the positive charges associated with ionized donor sites (<math>D^+</math> charges) are mobile and can propagate through the IR-active layer via the mechanism of hopping between occupied (<math>D^0</math>) and vacant (<math>D^+</math>) neighboring sites. A positive bias to the transparent contact creates a field that drives the pre-existing <math>D^+</math> charges towards the substrate, while the undoped blocking layer prevents the injection of new <math>D^+</math> charges. A region depleted of <math>D^+</math> charges is therefore created, with a width depending on the applied bias and on the compensating acceptor concentration.</p>
p-n junction photodiode		<p>This is the most widely used photovoltaic detector but is rather rarely used as a THz detector. Photons with energy greater than the energy gap create electron-hole pairs in the material on both sides of the junction. By diffusion, the electrons and holes generated within a diffusion length from the junction reach the space-charge region where they are separated by the strong electric field; minority carriers become majority carriers on the other side. This way a photocurrent is generated causing a change in voltage across the open-circuit cell or a current to flow in the short-circuited case. The limiting noise level of photodiodes can ideally be <math>\sqrt{2}</math> times lower than that of the photoconductor, due to the absence of recombination noise. Response times are generally limited by device capacitance and detector-circuit resistance.</p>

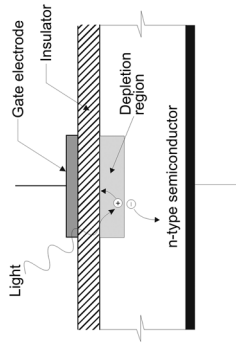


nBn detector



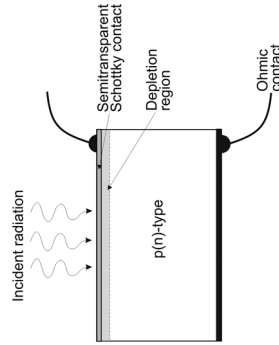
The nBn detector consists of a narrow-gap n-type absorber layer (AL), a thin wide-gap barrier layer (BL), and a narrow-gap n-type contact layer (CL). The thin wide-gap BL presents a large barrier in the conduction band that eliminates electron flow. Current through the nBn detector relies on transport of mobile holes through drift and diffusion in the BL between the two n-type narrow-gap regions. Effectively, the nBn detector is designed to reduce the dark current (generation-recombination current originating within the depletion layer) and noise without impeding the photocurrent (signal). In particular, the barrier serves to reduce the surface leakage current. The nBn detector operates as a unipolar unity-gain detector, and this design can be stated as a hybrid between photoconductor and photodiode.

Metal-insulator-semiconductor (MIS) photodiode



The MIS device consists of a metal gate separated from a semiconductor surface by an insulator (I). By applying a negative voltage to the metal electrode, electrons are repelled from the I-S interface, creating a depletion region. When incident photons create hole-electron pairs, the minority carriers drift away to the depletion region and the volume of the depletion region shrinks. The total amount of charge that a photogate can collect is defined as its well capacity. The total well capacity is decided by the gate bias, the insulator thickness, the area of the electrodes, and the background doping of the semiconductor. Numerous such photogates with proper clocking sequence form a CCD imaging array.

Schottky barrier photodiode



Schottky barrier photodiodes reveal some advantages over p-n junction photodiodes: fabrication simplicity (deposition of metal barrier on n(p)-semiconductor), absence of high-temperature diffusion processes, and high speed of response. Since it is a majority carrier device, minority carrier storage and removal problems do not exist, and therefore higher bandwidths can be expected. The thermionic emission process in a Schottky barrier is much more efficient than the diffusion process, and therefore for a given built-in voltage, the saturation current in a Schottky diode is several orders of magnitude higher than in the p-n junction.

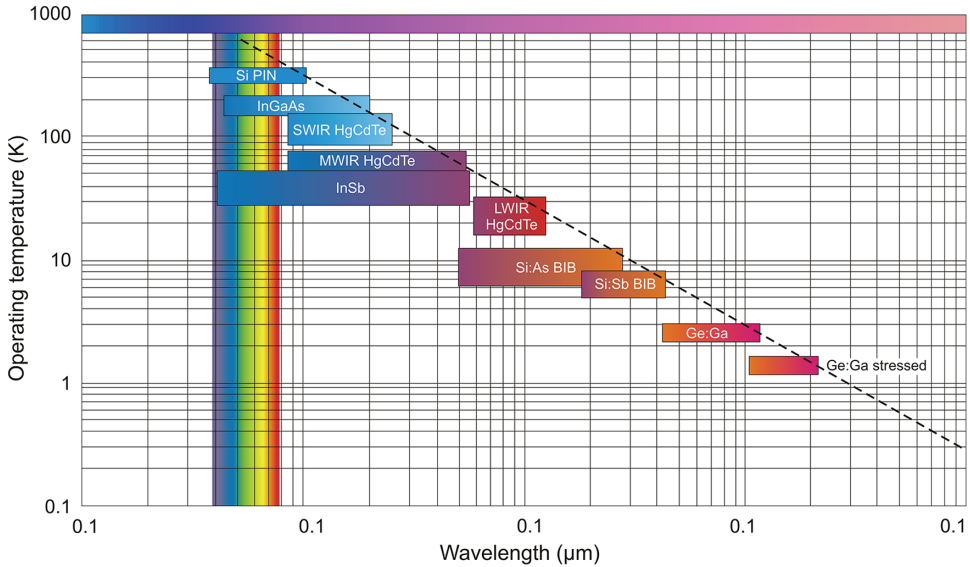


**Figure 1.5** Operating temperatures for low-background material systems with their spectral band of greatest sensitivity. The dashed line indicates the trend toward lower operating temperature for longer-wavelength detection (adapted from Ref. 3).

difference between intrinsic and extrinsic detectors is that extrinsic detectors require much cooling to achieve high sensitivity at a given spectral response cutoff in comparison with intrinsic detectors. Low-temperature operation is associated with longer-wavelength sensitivity in order to suppress noise due to thermally induced transitions between close-lying energy levels. Intrinsic detectors are most common at the short wavelengths, below 20  $\mu\text{m}$ . In the longer-wavelength region the photoconductors are operated in extrinsic mode. One advantage of photoconductors is their current gain, which is equal to the recombination time divided by the majority-carrier transit time. This current gain leads to higher responsivity than is possible with nonavalanching photovoltaic detectors. However, serious problem of photoconductors operated at low temperature is nonuniformity of detector element due to recombination mechanisms at the electrical contacts and its dependence on electrical bias.

Recently, interfacial workfunction internal photoemission detectors, quantum well and quantum dot detectors, which can be included to extrinsic photoconductors, have been proposed especially for IR and THz spectral bands.<sup>3</sup> The very fast time response of quantum well and quantum dot semiconductor detectors make them attractive for heterodyne detection.

## 1.2.2 Thermal detectors

The second class of detectors is composed of thermal detectors. In a thermal detector shown schematically in Fig. 1.6, the incident radiation is absorbed to

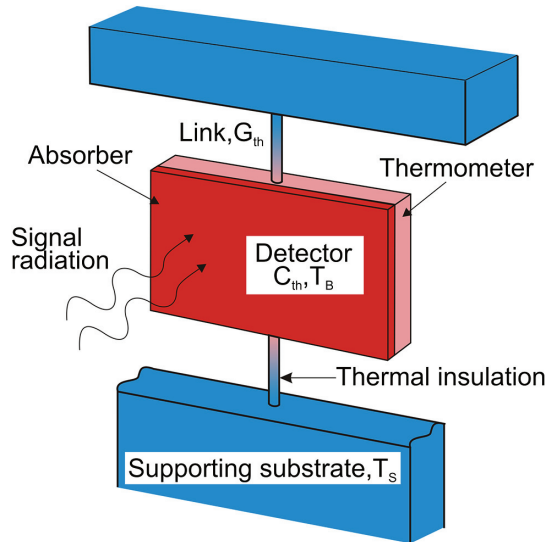


**Figure 1.6** Schematic diagram of thermal detector (adapted from Ref. 3).

change the material temperature, and the resultant change in some physical property is used to generate an electrical output. The detector is suspended on lags, which are connected to the heat sink. The signal does not depend upon the photonic nature of the incident radiation. Thus, thermal effects are generally wavelength independent [see Fig. 1.4(a)]; the signal depends upon the radiant power (or its rate of change) but not upon its spectral content. Since the radiation can be absorbed in a black surface coating, the spectral response can be very broad. Attention is directed toward three approaches that have found the greatest utility in infrared technology, namely, bolometers, pyroelectric, and thermoelectric effects. The thermopile is one of the oldest IR detectors, and is a collection of thermocouples connected in series in order to achieve better temperature sensitivity. In pyroelectric detectors a change in the internal electrical polarization is measured, whereas in the case of thermistor bolometers a change in the electrical resistance is measured. For a long time, thermopiles were slow, insensitive, bulky, and costly devices. But with developments in semiconductor technology, thermopiles can be optimized for specific applications. Recently, thanks to conventional complementary metal-oxide semiconductor (CMOS) processes, the thermopile's on-chip circuitry technology has opened the door to mass production.

Usually a bolometer is a thin, blackened flake or slab, whose impedance is highly temperature dependent. Bolometers may be divided into several types. The most commonly used are the metal, the thermistor, and the semiconductor bolometers. A fourth type is the superconducting bolometer. This bolometer operates on a conductivity transition in which the resistance changes

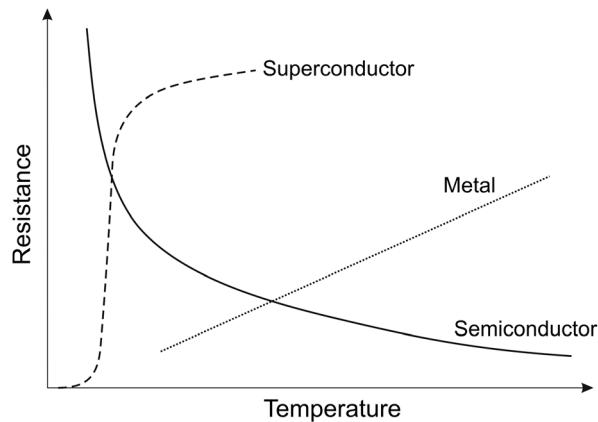


**Figure 1.7** Temperature dependence of resistance of three bolometer material types.

dramatically over the transition temperature range. Figure 1.7 shows schematically the temperature dependence of resistance of different types of bolometers.

Many types of thermal detectors are operated in wide spectral range of electromagnetic radiation. The operation principles of thermal detectors are briefly described in Table 1.2.

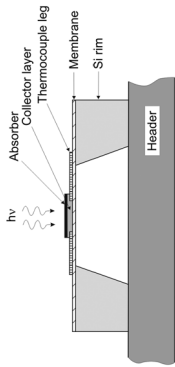
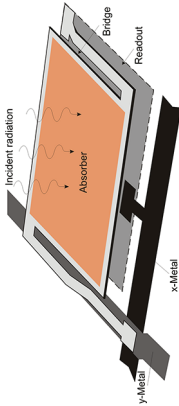
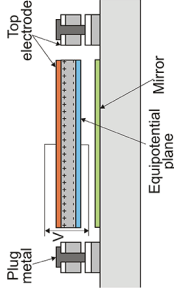
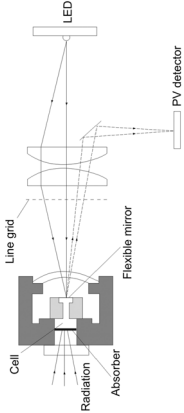
Microbolometer detectors are now produced in larger volumes than all other IR array technologies together. At present,  $\text{VO}_x$  microbolometer arrays are clearly the most used technology for uncooled detectors.  $\text{VO}_x$  wins the battle between the amorphous silicon bolometers and barium strontium titanate (BST) ferroelectric detectors.

### 1.3 Detector Figures of Merit

It is difficult to measure the performance characteristics of infrared detectors because of the large number of experimental variables involved. A variety of environmental, electrical, and radiometric parameters must be taken into account and carefully controlled. With the advent of large 2D detector arrays, detector testing has become even more complex and demanding.

This section is intended to serve as an introductory reference for the testing of infrared detectors. Numerous texts and journals cover this issue, including: *Infrared System Engineering*<sup>14</sup> by R. D. Hudson; *The Infrared Handbook*,<sup>15</sup> edited by W. L. Wolfe and G. J. Zissis; *The Infrared and Electro-Optical Systems Handbook*,<sup>16</sup> edited by W. D. Rogatto; and *Fundamentals of Infrared Detector Operation and Testing*<sup>17</sup> by J. D. Vincent, and second edition of Vincent's book.<sup>18</sup> In this chapter we have restricted our consideration to detectors whose output consists of an electrical signal that is proportional to the radiant signal power.

Table 1.2 Thermal detectors.

Mode of operation	Schematic of detector	Operation and properties
Thermopile		<p>The thermocouple is usually a thin, blackened flake connected thermally to the junction of two dissimilar metals or semiconductors. Heat absorbed by the flake causes a temperature rise of the junction, and hence a thermoelectric electromotive force is developed that can be measured. Although thermopiles are not as sensitive as bolometers and pyroelectric detectors, they will replace these in many applications due to their reliable characteristics and good cost/performance ratio. Thermocouples are widely used in spectroscopy.</p>
Bolometer Metal Semiconductor Superconductor Hot electron		<p>The bolometer is a resistive element constructed from a material with a very small thermal capacity and large temperature coefficient so that the absorbed radiation produces a large change in resistance. The change in resistance is like to the photoconductor, however, the basic detection mechanism is different. In the case of a bolometer, radiant power produces heat within the material, which in turn produces the resistance change. There is no direct photon-electron interaction. Initially, most bolometers were the thermistor type made from oxides of manganese, cobalt, or nickel. At present, microbolometers are fabricated in large-format arrays for thermal imaging applications. Some extremely sensitive low-temperature semiconductor and superconductor bolometers are used in the THz region.</p>
Pyroelectric detector		<p>The pyroelectric detector can be considered as a small capacitor with two conducting electrodes mounted perpendicularly to the direction of spontaneous polarization. During incident of radiation, the change in polarization appears as a charge on the capacitor and a current is generated, the magnitude of which depends on the temperature rise and the pyroelectric coefficient of the material. The signal, however, must be chopped or modulated. The detector sensitivity is limited either by amplifier noise or by loss-tangent noise. Response speed can be engineered making pyroelectric detectors useful for fast laser pulse detection, however with proportional decrease in sensitivity.</p>
Golay cell		<p>The Golay cell consists of a hermetically sealed container filled with gas (usually xenon for its low thermal conductivity) and arranged so that expansion of the gas under heating by a photon signal distorts a flexible membrane on which a mirror is mounted. The movement of the mirror is used to deflect a beam of light shinning on a photocell and so producing a change in the photocell current as the output. In modern Golay cells the photocell is replaced by a solid-state photodiode and light-emitting diode is used for illumination. The performance of the Golay cell is only limited by the temperature noise associated with the thermal exchange between the absorbing film and the detector gas, consequently the detector can be extremely sensitive with <math>D^* \approx 3 \times 10^9 \text{ cm Hz}^{1/2}\text{W}^{-1}</math>, and responsivities of <math>10^5</math> to <math>10^6 \text{ V/W}</math>. The response time is quite long, typically 15 msec.</p>

### 1.3.1 Responsivity

The responsivity of an infrared detector is defined as the ratio of the root mean square (rms) value of the fundamental component of the electrical output signal of the detector to the rms value of the fundamental component of the input radiation power. The units of responsivity are volts per watt (V/W) or amperes per watt (amp/W).

The voltage (or analogous current) spectral responsivity is given by

$$R_v(\lambda, f) = \frac{V_s}{\Phi_e(\lambda)}, \quad (1.2)$$

where  $V_s$  is the signal voltage due to  $\Phi_e$ , and  $\Phi_e(\lambda)$  is the spectral radiant incident power (in W).

An alternative to the above monochromatic quality, the blackbody responsivity, is defined by the equation

$$R_v(T, f) = \frac{V_s}{\int_0^\infty \Phi_e(\lambda) d\lambda}, \quad (1.3)$$

where the incident radiant power is the integral over all wavelengths of the spectral density of power distribution  $\Phi_e(\lambda)$  from a blackbody. The responsivity is usually a function of the bias voltage, the operating electrical frequency, and the wavelength.

### 1.3.2 Noise equivalent power

The noise equivalent power (*NEP*) is the incident power on the detector generating a signal output equal to the rms noise output. Stated another way, the *NEP* is the signal level that produces a signal-to-noise ratio (SNR) of 1. It can be written in terms of responsivity:

$$NEP = \frac{V_n}{R_v} = \frac{I_n}{R_i}. \quad (1.4)$$

The unit of *NEP* is watts.

The *NEP* is also quoted for a fixed reference bandwidth, which is often assumed to be 1 Hz. This “*NEP* per unit bandwidth” has a unit of watts per square root hertz (W/Hz<sup>1/2</sup>).

### 1.3.3 Detectivity

The detectivity *D* is the reciprocal of *NEP*:

$$D = \frac{1}{NEP}. \quad (1.5)$$

It was found by Jones<sup>19</sup> that for many detectors the *NEP* is proportional to the square root of the detector signal that is proportional to the detector area  $A_d$ . This means that both *NEP* and detectivity are functions of electrical bandwidth and detector area, so a normalized detectivity  $D^*$  (or *D*-star) suggested by Jones<sup>19,20</sup> is defined as

$$D^* = D(A_d \Delta f)^{1/2} = \frac{(A_d \Delta f)^{1/2}}{NEP}. \quad (1.6)$$

The importance of  $D^*$  is that this figure of merit permits comparison of detectors of the same type, but having different areas. Either a spectral or blackbody  $D^*$  can be defined in terms of the corresponding type of *NEP*.

Useful equivalent expressions to Eq. (1.6) include:

$$D^* = \frac{D(A_d \Delta f)^{1/2}}{V_n} R_v = \frac{D(A_d \Delta f)^{1/2}}{I_n} R_i = \frac{D(A_d \Delta f)^{1/2}}{\Phi_e} (SNR), \quad (1.7)$$

where  $D^*$  is defined as the rms SNR in a 1-Hz bandwidth per unit rms incident radiant power per square root of detector area.  $D^*$  is expressed in units of  $\text{cm Hz}^{1/2} \text{W}^{-1}$ , which recently has been referred to as “Jones.”

Spectral detectivity curves for a number of commercially available IR detectors are shown in Fig. 1.8. Interest has focused mainly on the two atmospheric windows 3–5  $\mu\text{m}$  (MWIR) and 8–14  $\mu\text{m}$  (LWIR) (atmospheric transmission is the highest in these bands and the emissivity maximum of the objects at  $T \approx 300 \text{ K}$  is at the wavelength  $\lambda \approx 10 \mu\text{m}$ ), although in recent years there has been increasing interest in longer wavelengths stimulated by space applications. The spectral character of the background is influenced by the transmission of the atmosphere that controls the spectral ranges of the infrared for which the detector may be used when operating in the atmosphere.

### 1.3.4 Quantum efficiency

A signal whose photon energy is sufficient to generate photocarriers will continuously lose energy as the optical field propagates through the semiconductor. Inside the semiconductor, the field decays exponentially as energy is transferred to the photocarriers. The material can be characterized by an absorption length  $\alpha$  and a penetration depth  $1/\alpha$ . Penetration depth is the point at which  $1/e$  of the optical signal power remains.

The power absorbed in the semiconductor as a function of position within the material is then

$$P_a = P_i(1 - r)(1 - e^{-\alpha x}). \quad (1.8)$$

The number of photons absorbed is the power (in watts) divided by the photon energy ( $E = h\nu$ ). If each absorbed photon generates a photocarrier,



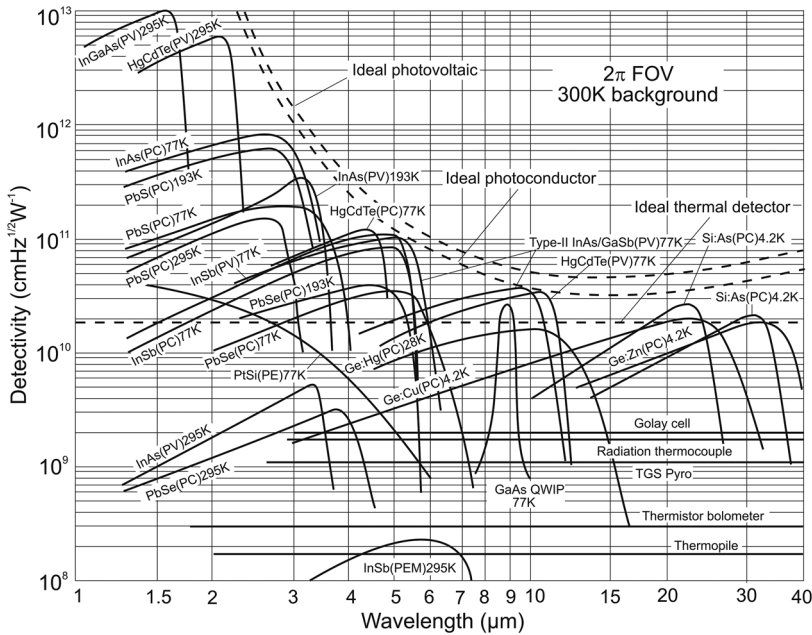


**Figure 1.8** Comparison of the  $D$  of various commercially available infrared detectors when operated at the indicated temperature. The chopping frequency is 1000 Hz for all detectors except the thermopile (10 Hz), thermocouple (10 Hz), thermistor bolometer (10 Hz), Golay cell (10 Hz), and pyroelectric detector (10 Hz). Each detector is assumed to view a hemispherical surround at a temperature of 300 K. Theoretical curves for the background-limited  $D$  for ideal photovoltaic and photoconductive detectors and thermal detectors are also shown (adapted from Ref. 3).

the number of photocarriers generated per number of incident photons for a specific semiconductor with reflectivity  $r$  is given by

$$\eta(x) = (1 - r)(1 - e^{-\alpha x}), \quad (1.9)$$

where  $0 \leq \eta \leq 1$  is a definition for the detector's quantum efficiency as the number of electron-hole pairs generated per incident photon.

Figure 1.9 shows the quantum efficiency of some of the detector materials used to fabricate arrays of ultraviolet (UV), visible, and infrared detectors. Photocathodes and AlGaIn detectors are being developed in the UV region. Silicon p-i-n diodes are shown with and without antireflection coating. Lead salts (PbS and PbSe) have intermediate quantum efficiencies, while PtSi Schottky barrier types and quantum well infrared photodetectors (QWIPs) have low values. InSb can respond from the near UV out to 5.5  $\mu\text{m}$  at 80 K. A suitable detector material for the near-IR (1.0–1.7  $\mu\text{m}$ ) spectral range is InGaAs lattice matched to the InP. Various HgCdTe alloys, in both photovoltaic and photoconductive configurations, cover from 0.7  $\mu\text{m}$  to over 20  $\mu\text{m}$ . InAs/GaSb strained layer superlattices have emerged as an alternative

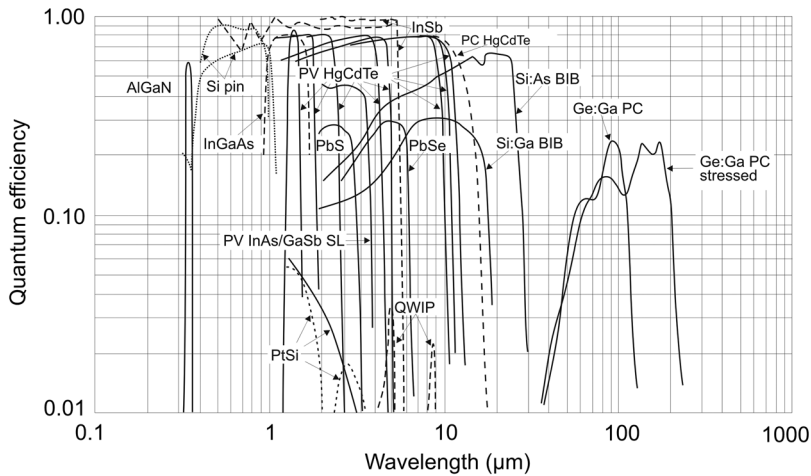


**Figure 1.9** Quantum efficiency of different detectors.

to the HgCdTe. Impurity-doped (Sb, As, and Ga) silicon BIB detectors operating at 10 K have a spectral response cutoff in the range of 16– to 30- $\mu\text{m}$ . Impurity-doped Ge detectors can extend the response out to 100–200  $\mu\text{m}$ .

#### 1.4 Fundamental Detector Performance Limits

In general, the detector can be considered as a slab of homogeneous semiconductor with actual “electrical” area  $A_e$ , thickness  $t$ , and volume  $A_e t$  (see Fig. 1.10). Usually, the optical and electrical areas of the device are the same or similar. However, the use of some kind of optical concentrator can increase the  $A_o/A_e$  ratio by a large factor.

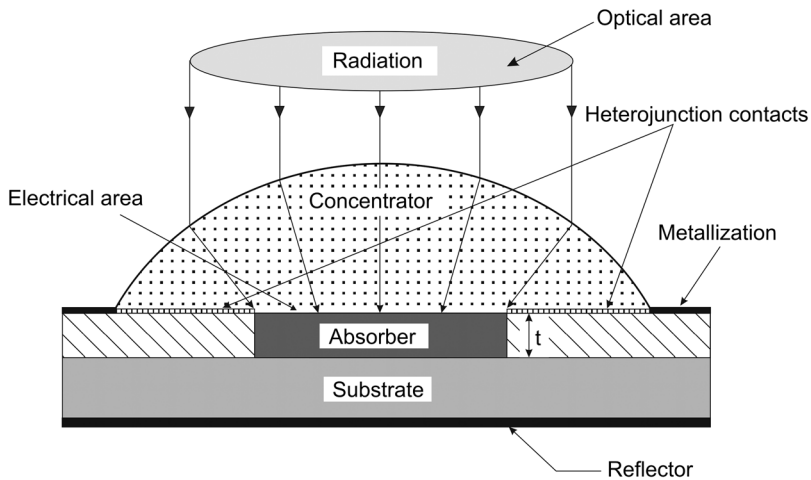


**Figure 1.10** Model of a photodetector (adapted from Ref. 3).

The detectivity  $D^*$  of an infrared photodetector is limited by generation and recombination rates  $G$  and  $R$  (in  $\text{m}^{-6}\text{s}^{-1}$ ) in the active region of the device.<sup>21</sup> It can be expressed as

$$D^* = \frac{\lambda}{2^{1/2}hc(G+R)^{1/2}} \left(\frac{A_o}{A_e}\right) \frac{\eta}{t^{1/2}}, \quad (1.10)$$

where  $\lambda$  is the wavelength,  $h$  is Planck's constant,  $c$  is the velocity of light, and  $\eta$  is the quantum efficiency.

For a given wavelength and operating temperature, the highest performance can be obtained by maximizing the ratio of the quantum efficiency to the square root of the sum of the sheet thermal generation and recombination rates  $\eta/[(G+R)t]^{1/2}$ . This means that high quantum efficiency must be obtained with a thin device.

A possible way to improve the performance of IR detectors is to reduce the physical volume of the semiconductor, thus reducing the amount of thermal generation. However, this must be achieved without decrease in quantum efficiency, optical area, and field of view (FOV) of the detector.

At equilibrium, the generation and recombination rates are equal. If we further assume  $A_e = A_o$ , the detectivity of an optimized infrared photodetector is limited by thermal processes in the active region of the device. It can be expressed as

$$D^* = 0.31 \frac{\lambda}{hc} k \left(\frac{\alpha}{G}\right)^{1/2}, \quad (1.11)$$

where  $1 \leq k \leq 2$  and is dependent on the contribution of recombination and backside reflection. The  $k$ -coefficient can be modified by using more sophisticated coupling of the detector with IR radiation, e.g., using photonic crystals or surface plasmon-polaritons.

The ratio of the absorption coefficient to the thermal generation rate,  $\alpha/G$ , is the fundamental figure of merit of any material intended for infrared photodetection. The  $\alpha/G$  ratio versus temperature for various material systems capable of bandgap tuning is shown in Fig. 1.11 for a hypothetical energy gap equal to 0.25 eV ( $\lambda = 5 \mu\text{m}$ ) [Fig. 1.11(a)] and 0.124 eV ( $\lambda = 10 \mu\text{m}$ ) [Fig. 1.11(b)]. Procedures used in calculations of  $\alpha/G$  for different material systems are given in Ref. 22. Analysis shows that narrow-gap semiconductors are more suitable for high-temperature photodetectors in comparison to competing technologies such as extrinsic devices, QWIP (quantum well IR photodetector) and QDIP (quantum dot IR photodetector) devices. The main reason for the high performance of intrinsic photodetectors is the high density of states in the valence and conduction bands, which results in strong absorption of infrared radiation. Figure 1.11(b) predicts that a recently emerging

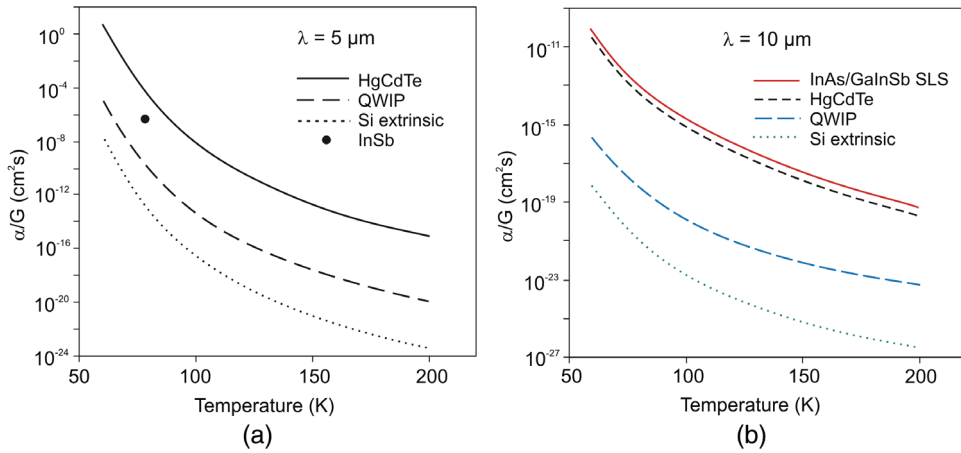


**Figure 1.11**  $\alpha/G$  ratio versus temperature for (a) MWIR ( $\lambda = 5 \mu\text{m}$ ) and (b) LWIR ( $\lambda = 10 \mu\text{m}$ ) photodetectors based on HgCdTe, QWIP, Si extrinsic, and type-II superlattice (for LWIR only) material technology (adapted from Ref. 3).

competing IR material, type-II superlattice, is the most efficient material technology for IR detection in the long-wavelength region, theoretically perhaps even better than HgCdTe if the influence of the Shockley–Read–Hall lifetime is not considered. It is characterized by a high absorption coefficient and relatively low fundamental (band-to-band) thermal generation rate. However, this theoretical prediction has not been confirmed by experimental data. It is also worth noting that theoretically AlGaAs/GaAs QWIP is also a better material than extrinsic silicon.

The ultimate performance of infrared detectors is reached when the detector and amplifier noise are low compared to the photon noise. The photon noise is fundamental in the sense that it arises not from any imperfection in the detector or its associated electronics but rather from the detection process itself, as a result of the discrete nature of the radiation field. The radiation falling on the detector is a composite of that from the target and that from the background. The practical operating limit for most infrared detectors is not the signal fluctuation limit but the background fluctuation limit, also known as the background-limited infrared photodetector (BLIP) limit.

The expression for shot noise can be used to derive the BLIP detectivity,

$$D_{BLIP}^*(\lambda, T) = \frac{\lambda}{hc} k \left( \frac{\eta}{2\Phi_B} \right)^{1/2}, \quad (1.12)$$

where  $\eta$  is the quantum efficiency, and  $\Phi_B$  is the total background photon flux density reaching the detector, denoted as

$$\Phi_B = \sin^2(\theta/2) \int_0^{\lambda_c} \Phi(\lambda, T_B) d\lambda, \quad (1.13)$$

where  $\theta$  is the detector field of view angle.

Planck's photon emittance (in units of photons  $\text{cm}^{-2}\text{s}^{-1} \mu\text{m}^{-1}$ ) at temperature  $T_B$  is given by

$$\Phi(\lambda, T_B) = \frac{2\pi c}{\lambda^4 [\exp(hc/\lambda k T_B) - 1]} = \frac{1.885 \times 10^{23}}{\lambda^4 [\exp(14.388/\lambda k T_B) - 1]}. \quad (1.14)$$

Equation (1.12) holds for photovoltaic detectors, which are shot-noise limited. Photoconductive detectors that are generation-recombination noise limited have a lower  $D_{BLIP}^*$  by a factor of  $2^{1/2}$ :

$$D_{BLIP}^*(\lambda, f) = \frac{\lambda}{2 hc} k \left( \frac{\eta}{\Phi_B} \right)^{1/2}. \quad (1.15)$$

Once background-limited performance is reached, quantum efficiency  $\eta$  is the only detector parameter that can influence detector's performance.

Figure 1.12 shows the peak spectral detectivity of a background-limited photodetector operating at 300, 230, and 200 K, versus the wavelength calculated for 300 K background radiation and hemispherical FOV ( $\theta = 90$  deg). The minimum  $D_{BLIP}^*$  (300 K) occurs at  $14 \mu\text{m}$  and equals  $4.6 \times 10^{10} \text{ cm Hz}^{1/2}/\text{W}$ . For some photodetectors that operate at near

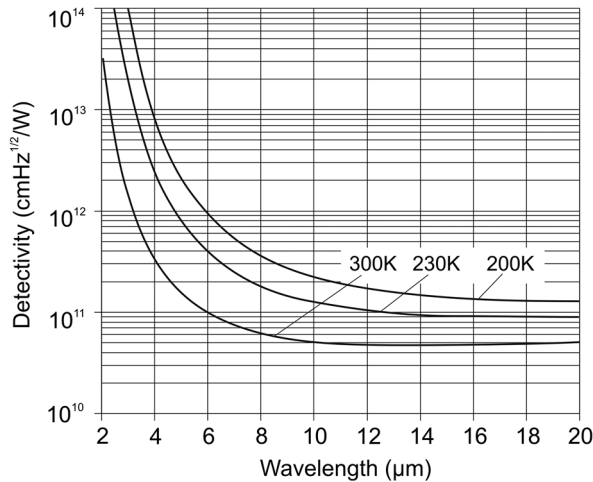


**Figure 1.12** Calculated spectral detectivities of a photodetector limited by the hemispherical FOV background radiation of 300 K as a function of the peak wavelength for detector operating temperatures of 300, 230, and 200 K (reprinted from Ref. 23).

equilibrium conditions, such as non-sweep-out photoconductors, the recombination rate is equal to the generation rate. For these detectors the contribution of recombination to the noise will reduce  $D_{BLIP}^*$  by a factor of  $2^{1/2}$ . Note that  $D_{BLIP}^*$  does not depend on area and the  $A_o/A_e$  ratio. As a consequence, the background-limited performance cannot be improved by making  $A_o/A_e$  large.

The highest performance possible will be obtained by the ideal detector with unity quantum efficiency and ideal spectral responsivity [ $R(\lambda)$  increases with wavelength to the cutoff wavelength  $\lambda_c$  at which the responsivity drops to zero]. This limiting performance is of interest for comparison with actual detectors.

The detectivity of BLIP detectors can be improved by reducing the background photon flux  $\Phi_B$ . Practically, there are two ways to do this: a cooled or reflective spectral filter to limit the spectral band or a cooled shield to limit the angular field of view of the detector (as described above). The former eliminates background radiation from spectral regions in which the detector need not respond. The best detectors yield background-limited detectivities in quite narrow fields of view.

## 1.5 Performance of Focal Plane Arrays

This section discusses concepts associated with the performance of focal plane arrays (FPAs). For arrays the relevant figure of merit for determining the ultimate performance is not the detectivity  $D^*$ , but the noise equivalent difference temperature (*NEDT*) and the modulation transfer function (*MTF*). *NEDT* and *MTF* are considered as the primary performance metrics to thermal imaging systems: thermal sensitivity and spatial resolution. Thermal sensitivity is concerned with the minimum temperature difference that can be discerned above the noise level. The *MTF* concerns the spatial resolution and answers the question of how small an object can be and still be imaged by the system. The general approach of system performance is given by Lloyd in his fundamental monograph.<sup>24</sup>

### 1.5.1 Modulation transfer function

The modulation transfer function (*MTF*) expresses the ability of an imaging system to faithfully image a given object; it quantifies the ability of the system to resolve or transfer spatial frequencies.<sup>25</sup> Consider a bar pattern with a cross-section of each bar being a sine wave. Since the image of a sine wave light distribution is always a sine wave, the image is always a sine wave independent of the other effects in the imaging system, such as aberrations.

Usually, imaging systems have no difficulty in reproducing the bar pattern when the bar pattern is sparsely spaced. However, an imaging system reaches

its limit when the features of the bar pattern get closer and closer together. When the imaging system reaches this limit, the contrast or the modulation  $M$  is defined as

$$M = \frac{E_{\max} - E_{\min}}{E_{\max} + E_{\min}}, \quad (1.16)$$

where  $E$  is the irradiance. Once the modulation of an image is measured experimentally, the  $MTF$  of the imaging system can be calculated for that spatial frequency using

$$MTF = \frac{M_{\text{image}}}{M_{\text{object}}}. \quad (1.17)$$

The system  $MTF$  is dominated by the optics, detector, and display  $MTFs$  and can be cascaded by simply multiplying the  $MTF$  components to obtain the  $MTF$  of the combination. In spatial frequency terms, the  $MTF$  of an imaging system at a particular operating wavelength is dominated by limits set by the size of the detector and the aperture of the optics. More details about this issue is given in section 9.2.

### 1.5.2 Noise equivalent difference temperature

Noise equivalent difference temperature ( $NEDT$ ) is a figure of merit for thermal imagers that is commonly reported. In spite of its widespread use in infrared literature, it is applied to different systems, in different conditions, and with different meanings.<sup>26</sup>

$NEDT$  of a detector represents the temperature change, for incident radiation, that gives an output signal equal to the rms noise level. While normally thought of as a system parameter, detector  $NEDT$  and system  $NEDT$  are the same except for system losses.  $NEDT$  is defined as

$$NEDT = \frac{V_n(\partial T/\partial\Phi)}{(\partial V_s/\partial\Phi)} = V_n \frac{\Delta T}{\Delta V_s}, \quad (1.18)$$

where  $V_n$  is the rms noise,  $\Phi$  is the spectral photon flux density (photons/cm<sup>2</sup>s) incident on a focal plane, and  $\Delta V_s$  is the signal measured for the temperature difference  $\Delta T$ .

We follow Kinch<sup>27</sup> further to obtain useful equations for noise equivalent irradiance ( $NEI$ ) and  $NEDT$ , used for estimation of detector performance (see e.g., section 6.6).

In modern IR FPAs the current generated in a biased photon detector is integrated onto a capacitive node with a carrier well capacity of  $N_w$ . For an ideal system, in absence of excess noise, the detection limit of the node is



achieved when a minimum detectable signal flux  $\Delta\Phi$  creates a signal equal shot noise on the node:

$$\Delta\Phi\eta A_d\tau_{\text{int}} = \sqrt{N_w} = \sqrt{\frac{(J_{\text{dark}} + J_{\Phi})A_d\tau_{\text{int}}}{q}}, \quad (1.19)$$

where  $\eta$  is the detector collection efficiency,  $A_d$  is the detector area,  $\tau_{\text{int}}$  is the integration time,  $J_{\text{dark}}$  is the detector dark current, and  $J_{\Phi}$  is the flux current.

Associated with *NE $\Delta\Phi$*  is the other critical parameter, the so-called noise equivalent flux (*NE $\Delta\Phi$* ). This parameter is defined for spectral regions in which the thermal background flux does not dominate. By equating the minimum detectable signal to the integrated current noise, we have

$$\eta\Phi_s A_d\tau_{\text{int}} = \sqrt{\frac{(J_{\text{dark}} + J_{\Phi})A_d\tau_{\text{int}}}{q}}, \quad (1.20)$$

giving

$$NE\Delta\Phi = \frac{1}{\eta} \sqrt{\frac{J_{\text{dark}} + J_{\Phi}}{qA_d\tau_{\text{int}}}}. \quad (1.21)$$

This can be converted to a noise equivalent irradiance (*NEI*), which is defined as the minimum observable flux power incident on the system aperture, by renormalizing the incident flux density on the detector to the system aperture area  $A_{\text{opt}}$ . The *NEI* is given by

$$NEI = NE\Delta\Phi \frac{A_d h\nu}{A_{\text{opt}}}, \quad (1.22)$$

where monochromatic radiation of energy  $h\nu$  is assumed.

*NEI* [photons/(cm<sup>2</sup>sec)] is the signal flux level at which the signal produces the same output as the noise present in the detector. This unit is useful because it directly gives the photon flux above which the detector will be photon-noise limited.

For high-background-flux conditions, the signal flux can be defined as  $\Delta\Phi = \Delta T(d\Phi_B/dT)$ . Thus, for shot noise, substituting in Eq. (1.19), we have

$$\eta\Delta T \frac{d\Phi_B}{dT} = \sqrt{\frac{J_{\text{dark}} + J_{\Phi}}{qA_d\tau_{\text{int}}}}. \quad (1.23)$$

Finally, after some re-arrangement,

$$NEDT = \frac{1 + (J_{dark}/J_{\Phi})}{\sqrt{N_w C}}, \quad (1.24)$$

where  $C = (d\Phi_B/dT)/\Phi_B$  is the scene contrast through the optics. In deriving Eq. (1.24) it was assumed that the optics transmission is unity, and that the cold shield of the detector is not contributing flux. This is reasonable at low detector temperatures but not at higher operating temperatures. At higher temperatures the scene contrast is defined in terms of the signal flux coming through the optics, whereas the flux current is defined by the total flux through the optics and the flux from the cold shield.

### 1.5.3 Other issues

Infrared photodetectors are typically operated at cryogenic temperatures to decrease the noise of the detector arising from various mechanisms associated with the narrow bandgap. There are considerable efforts to decrease system cost, size, weight, and power consumption, to increase the operating temperature in so-called high-operating-temperature (HOT) detectors. Increasing the operating temperature of the detector reduces the cooling load, allowing more compact cooling systems with higher efficiency. Because the cost of the optics made from Ge (the standard material for IR optics) rises approximately with the square of the lens diameter, the reduction of the pixel size results in a significantly reduced cost of the optics. In addition, the reduction in pixel size allows for a larger number of FPAs to be fabricated on each wafer.

Pixel reduction is also needed to increase the detection and identification range of infrared imaging systems. It appears that, e.g., the detection range of many uncooled IR imaging systems is limited by pixel resolution rather than sensitivity. Figure 1.13 presents a trade-off analysis of the detection range and

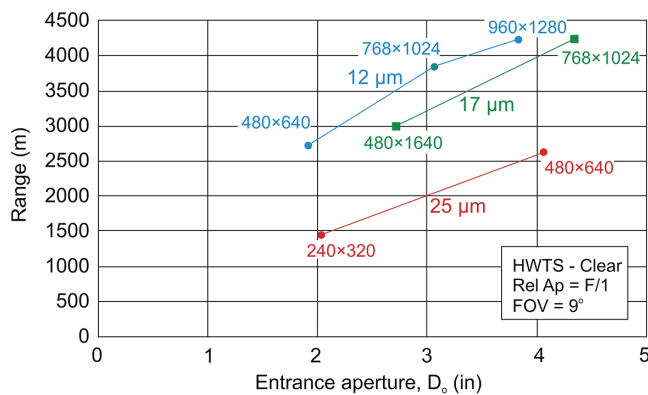


**Figure 1.13** Calculated detection range as a function of sensor optics for increasing detector pixel size and format using NVESD NVTherm IP modeling, assuming a 35-mK  $NEDT$  ( $F/1$ , 30Hz) for all detectors (reprinted from Ref. 28).

sensor optics for a thermal weapon sight using the NVESD NVTherm IP model, assuming a detector sensitivity of 35-mK *NETD* ( $F/1$ , 30 Hz) for the 25-, 17-, and 12- $\mu\text{m}$  pitch pixel of uncooled FPAs. The advantages of small pixel pitch and large-format FPAs are obvious. By switching to smaller pitch and larger format detectors, the detection range of a weapon sight increases significantly with a fixed optical entrance aperture.

Key challenges in realizing ultimate pixel dimensions in FPA design including dark current, pixel hybridization, pixel delineation, and unit cell readout capacity are considered in Refs. 27 and 29, and Section 9.2 of this book.

It is interesting to consider the performance requirements of near-room-temperature photodetectors for thermal cameras. It can be shown<sup>3</sup> that the thermal resolution of infrared thermal systems is characterized by the equation

$$NETD = \frac{4(F/\#)^2 \Delta f^{1/2}}{A_d^{1/2} t_{opt}} \left[ \int_{\lambda_a}^{\lambda_b} \frac{dM}{dT} D^*(\lambda) d\lambda \right], \quad (1.25)$$

where  $F/\#$  is the optics f-number,  $\Delta f$  is the frequency band,  $A_d$  is the detector area,  $t_{opt}$  is the optics transmission, and  $M$  is the spectral emittance of the blackbody described by Planck's law.

As Eq. (1.25) shows, the thermal resolution improves with an increase in detector area. However, increasing detector area results in reduced spatial resolution. Hence, a reasonable compromise between the requirement of high thermal resolution and spatial resolution is necessary. Improvement of thermal resolution without detrimental effects on spatial resolution may be achieved by:

- an decrease of detector area combined with a corresponding decrease of the optics f-number,
- improved detector performance, and
- an increase in the number of detectors.

As was mentioned before, increasing the aperture is undesirable because it increases the size, mass, and price of an IR system. It is more appropriate to use a detector with higher detectivity. This can be achieved by better coupling of the detector with the incident radiation. Another possibility is the application of a multi-elemental sensor, which reduces each element bandwidth proportionally to the number of elements for the same frame rate and other parameters.

Figure 1.14 shows the dependence of detectivity on the cutoff wavelength for a photodetector thermal imager with a resolution of 0.1 K. Detectivities of  $1.9 \times 10^8 \text{ cm Hz}^{1/2}/\text{W}$ ,  $2.3 \times 10^8 \text{ cm Hz}^{1/2}/\text{W}$ , and  $2 \times 10^9 \text{ cm Hz}^{1/2}/\text{W}$  are necessary to obtain  $NETD = 0.1 \text{ K}$  for 10- $\mu\text{m}$ , 9- $\mu\text{m}$ , and 5- $\mu\text{m}$  cutoff wavelengths, respectively. The above estimations indicate that the ultimate

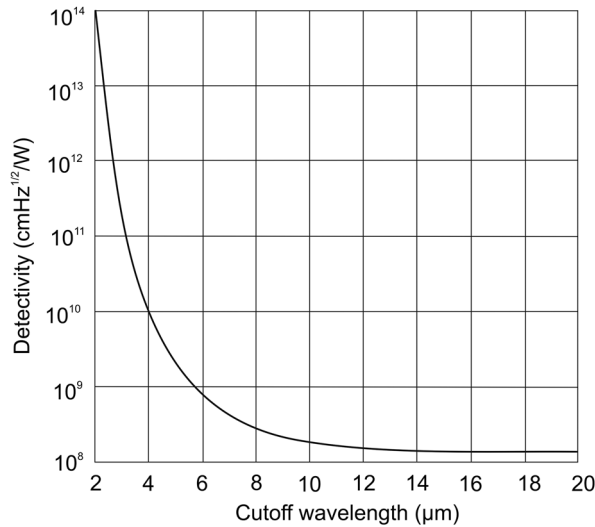


**Figure 1.14** Detectivity needed to obtain  $NEDT = 0.1$  K in a photon-counter detector thermal imager as a function of cutoff wavelength (reprinted from Ref. 23).

performance of the uncooled photodetectors is not sufficient to achieve a thermal resolution of 0.1 K. Thermal resolution below 0.1 K is achieved for staring thermal imagers containing thermal FPAs.

The previous considerations are valid assuming that the temporal noise of the detector is the main source of noise. However, this assertion is not true for staring arrays, where the nonuniformity of the detector response is a significant source of noise. This nonuniformity appears as a fixed-pattern noise (spatial noise) and is defined in various ways in the literature. The most common definition is that it is the dark signal nonuniformity arising from an electronic source (i.e., other than thermal generation of the dark current); e.g., clock breakthrough or from offset variations in row, column, or pixel amplifiers/switches. So, estimation of IR sensor performance must include a treatment of spatial noise that occurs when FPA nonuniformities cannot be compensated correctly.

Mooney et al.<sup>30</sup> have given a comprehensive discussion of the origin of spatial noise. The total noise of a staring array is the composite of the temporal noise and the spatial noise. The spatial noise is the residual nonuniformity  $u$  after application of nonuniformity compensation, multiplied by the signal electrons  $N$ . Photon noise, which equals  $N^{1/2}$ , is the dominant temporal noise for the high IR background signals for which spatial noise is significant. Then, the total  $NEDT$  is

$$NEDT_{total} = \frac{(N + u^2 N^2)^{1/2}}{\partial N / \partial T} = \frac{(1/N + u^2)^{1/2}}{(1/N)(\partial N / \partial T)}, \quad (1.26)$$

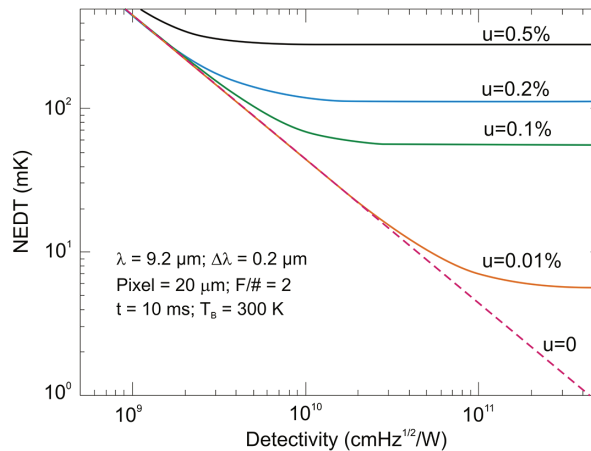


**Figure 1.15** *NEDT* as a function of detectivity. The effects of nonuniformity are included for  $u = 0.01\%$ ,  $0.1\%$ ,  $0.2\%$ , and  $0.5\%$ . Note that for  $D^* > 10^{10}$  cm Hz<sup>1/2</sup>/W, detectivity is not the relevant figure of merit 9 (adapted from Ref. 3).

where  $\partial N/\partial T$  is the signal change for a 1-K source temperature change. The denominator,  $(\partial N/\partial T)/N$ , is the fractional signal change for a 1-K source temperature change. This is the relative scene contrast.

The dependence of the total *NEDT* on detectivity for different residual nonuniformity is plotted in Fig. 1.15 for 300 K scene temperature and the set of parameters shown in the figure insert. When detectivity approaches a value above  $10^{10}$  cm Hz<sup>1/2</sup>/W, the FPA performance is uniformity-limited prior to correction and thus essentially independent of the detectivity. An improvement in nonuniformity from  $0.1\%$  to  $0.01\%$  after correction could lower the *NEDT* from 63 to 6.3 mK.

## References

1. R. J. Cashman, "Film-type infrared photoconductors," *Proc. IRE* **47**, 1471–1475 (1959).
2. E. Burstein, G. Pines, and N. Sclar, "Optical and photoconductive properties of silicon and germanium," in *Photoconductivity Conference at Atlantic City*, edited by R. Breckenbridge, B. Russell, and E. Hahn, Wiley, New York, pp. 353–413 (1956).
3. A. Rogalski, *Infrared Detectors*, 2<sup>nd</sup> edition, CRC Press, Boca Raton, Florida (2010).
4. R. A. Soref, "Extrinsic IR photoconductivity of Si doped with B, Al, Ga, P, As or Sb," *J. Appl. Phys.* **38**, 5201–5209 (1967).
5. W. S. Boyle and G. E. Smith, "Charge-coupled semiconductor devices," *Bell Syst. Tech. J.* **49**, 587–593 (1970).

6. F. Shepherd and A. Yang, "Silicon Schottky retinas for infrared imaging," *IEDM Tech. Dig.*, 310–313 (1973).
7. C. Hilsum and A. C. Rose-Innes, *Semiconducting III-V Compounds*, Pergamon Press, Oxford (1961).
8. J. Melngailis and T. C. Harman, "Single-crystal lead-tin chalcogenides," in *Semiconductors and Semimetals*, Vol. 5, edited by R. K. Willardson and A. C. Beer, Academic Press, New York, pp. 111–174 (1970).
9. T. C. Harman and J. Melngailis, "Narrow gap semiconductors," in *Applied Solid State Science*, Vol. 4, edited by R. Wolfe, Academic Press, New York, pp. 1–94 (1974).
10. W. D. Lawson, S. Nielson, E. H. Putley, and A. S. Young, "Preparation and properties of HgTe and mixed crystals of HgTe-CdTe," *J. Phys. Chem. Solids* 9, 325–329 (1959).
11. S. Krishna, "The infrared retina," *J. Phys. D: Appl. Phys.* 42, 234005 (2009).
12. A. Rogalski and F. Sizov, "Terahertz detectors and focal plane arrays," *Opto-Electr. Rev.* 19(3), 346–404 (2011).
13. D. Long, "Photovoltaic and photoconductive infrared detectors," in *Optical and Infrared Detectors*, edited by R. J. Keyes, Springer, Berlin, pp. 101–147 (1980).
14. R. D. Hudson, *Infrared System Engineering*, Wiley, New York (1969).
15. *The Infrared Handbook*, edited by W. I. Wolfe and G. J. Zissis, Office of Naval Research, Washington, D.C. (1985).
16. *The Infrared and Electro-Optical Systems Handbook*, edited by W. D. Rogatto, Infrared Information Analysis Center, Ann Arbor and SPIE Press, Bellingham, Washington (1993).
17. J. D. Vincent, *Fundamentals of Infrared Detector Operation and Testing*, Wiley, New York (1990).
18. J. D. Vincent, S. E. Hodges, J. Vampola, M. Stegall, and G. Pierce, *Fundamentals of Infrared and Visible Detector Operation and Testing*, Wiley, Hoboken, New Jersey (2016).
19. R. C. Jones, "Performance of detectors for visible and infrared radiation," in *Advances in Electronics*, Vol. 5, edited by L. Morton, Academic Press, New York, pp. 27–30 (1952).
20. R. C. Jones, "Phenomenological description of the response and detecting ability of radiation detectors," *Proc. IRE* 47, 1495–1502 (1959).
21. J. Piotrowski and A. Rogalski, Comment on "Temperature limits on infrared detectivities of InAs/In<sub>x</sub>Ga<sub>1-x</sub>Sb superlattices and bulk Hg<sub>1-x</sub>Cd<sub>x</sub>Te" [*J. Appl. Phys.* 74, 4774 (1993)], *J. Appl. Phys.* 80(4), 2542–2544 (1996).
22. A. Rogalski, "Quantum well photoconductors in infrared detector technology," *J. Appl. Phys.* 93, 4355 (2003).
23. J. Piotrowski and A. Rogalski, *High-Operating Temperature Infrared Photodetectors*, SPIE Press, Bellingham, Washington (2007) [doi: 10.1117/3.717228].

24. J. M. Lloyd, *Thermal Imaging Systems*, Plenum Press, New York (1975).
25. G. C. Holst, "Infrared imaging testing," in *The Infrared & Electro-Optical Systems Handbook*, Vol. 4 *Electro-Optical Systems Design, Analysis, and Testing*, edited by M. C. Dudzik, SPIE Press, Bellingham, Washington (1993).
26. J. M. Lopez-Alonso, "Noise equivalent temperature difference (NETD)," in *Encyclopedia of Optical Engineering*, edited by R. Driggers, Marcel Dekker Inc., New York, pp. 1466–1474 (2003).
27. M. A. Kinch, *State-of-the-Art Infrared Detector Technology*, SPIE Press, Bellingham, Washington (2014) [doi: 10.1117/3.1002766].
28. C. Li, G. Skidmore, C. Howard, E. Clarke, and C. J. Han, "Advancement in 17 micron pixel pitch uncooled focal plane arrays," *Proc. SPIE* **7298**, 72980S (2009) [doi: 10.1117/12.818189].
29. A. Rogalski, P. Martyniuk, and M. Kopytko, "Challenges of small-pixel infrared detectors: a review," *Rep. Prog. Phys.* **79**, 046501 (2016).
30. J. M. Mooney, F. D. Shepherd, W. S. Ewing, and J. Silverman, "Responsivity nonuniformity limited performance of infrared staring cameras," *Opt. Eng.* **28**, 1151 (1989) [doi: 10.1117/12.7977112].